Electronic- and vibrational-structure calculations in models of the compressed SiO_2 glass system

R. A. Murray*
Department of Physics and Astronomy, University of Kansas, Lawrence, Kansas 66045
and Department of Physics, University of Missouri–Kansas City, Kansas City, Missouri 64110-2499

W. Y. Ching
Department of Physics, University of Missouri–Kansas City, Kansas City, Missouri 64110-2499
(Received 3 June 1988)

The electronic and vibrational structures of normal and compressed SiO_2 glasses are studied using realistic continuous-random-network models with periodic boundaries. The electronic structure is calculated by the first-principles orthogonalized linear combination of atomic orbitals (OLCAO) method and the results are presented for density of states, band gaps, effective charges, and localization of wave functions as a function of density. The vibrational density of states, infrared absorption, and Raman spectra for these models are also calculated with use of a Keating-type potential and the bond-polarizability approximation. The results are, generally, in good agreement with experiments on both normal and "densified" a-SiO_2. In particular, the two Raman lines at 495 and 606 cm^{-1} are reproduced by our calculation in direct contrast to the paracrystalline theory of SiO_2 glass. Inspection of eigenvectors in conjunction with a detailed analysis of the bonding patterns of participating atoms indicate that specific Si—O—Si angles (close to those found in threefold or fourfold rings) are responsible for these modes.

I. INTRODUCTION

Over the years certain physical problems have proven too difficult or unwieldy to be solved by analytical means. One such problem is the structure of amorphous solids in general and silicate glasses in particular. Experimental methods such as x-ray diffraction, which yield exact atomic positions for crystals, can give only average atomic distances and angles for the glass phase. Also, theoretical techniques for determining the electronic and vibrational structures are hampered by the lack of realistic models. One way to resolve this problem associated with going from ambiguous experimental data to specific atomic arrangements is to reverse the approach. Physical observables can be calculated from the specific atomic positions of a realistic model structure and checked against experimental measurements. If two models give the same similar calculated results for one type of experiment (x-ray scattering, for example), then the calculated results for other experiments (like Raman scattering) can be used to distinguish which model is closer to the real system. The debate over how to explain the experimental scattering data in the amorphous SiO_2 (a-SiO_2) system has been brewing for the past 50 years. Recently the interpretation of infrared Raman scattering has further enhanced interest in this system. Also, the unusual properties of a-SiO_2 under pressure (such as bond-angle changes and densification) have been the subject of renewed experimental investigation. The illumination of these questions was the principal motivation behind the present study.

In 1936 Warren, Krutter, and Morningstar[1] used x-ray scattering to determine the local atomic-bonding patterns in silicate glasses. They used similarities between the basic atomic structures of the crystalline and amorphous phases to interpret the radial distribution functions (RDF) obtained from the scattering data. In this way, they were able to assign peaks in the RDF curves at 1.62, 2.65, and 3.2 Å to the mean Si-O, O-O, and Si-Si distances, respectively. The atomic structures seemed to be based on the SiO_4 tetrahedra found in most silicate crystals. In this type of system, each Si atom is bonded to four O atoms, and each O atom bonds to two Si atoms from different tetrahedra in a continuous fashion. This type of arrangement, where the units are linked in a nonperiodic fashion, is called a continuous random network (CRN) and was proposed in 1932 by Zachariasen[2] as the long-range structure for a-SiO_2. The CRN theory was criticized by some as being incapable of describing the glass formation from the melt.[3] Although the scattering experiment of Warren *et al.*[1] did not explicitly prove the validity of the CRN theory, they were in agreement with Zachariasen's predictions. Through the years, various researchers have studied the a-SiO_2 system through scattering experiments[4–7] and the CRN theory gradually became accepted. Recently the argument has erupted again, based on some observed features in the Raman spectra in a-SiO_2. Certain peaks in the Raman shifts for a-SiO_2 were interpreted by Phillips[8] as indicative of the presence of a paracrystalline atomic structure. That is, the atomic structure of a-SiO_2 is supposed to be represented by large (>60 Å diameter) crystalline clusters of β-cristoballite separated by material of higher defect concentration. The Raman peaks are supposed to be due to nonbridging oxygen (NBO) sites at the surface of

the cluster. The CRN position has been defended by Galeener[9,10] who has stated that the Raman peaks can be accounted for by specific ring structures in the CRN. Another aspect of the a-SiO_2 system that is not well understood is the behavior at high pressure. Like most materials, when a-SiO_2 is compressed there is a volume change and a corresponding increase in the mass density. If this compression is less than a certain threshold, then the density drops back to its precompressed value. However, if the glass is pressurized beyond the threshold, the density will remain at the elevated value even when the pressure is released. These increased densities are permanent and indicate that irreversible structural changes have taken place in the glass at the microscopic level.[11] Such glass is said to be "densified." The threshold at which a-SiO_2 becomes densified is approximately 90–100 kbar at room temperature[12–14] but can be lower if the compression is done at an elevated temperature. The maximum densification for the a-SiO_2 is usually thought to be 15–16% (Refs. 15 and 16) but Devine and Arndt[17] have reported densification as high as 24% at high temperature.

The work reported here consists of three parts. The first part describes the development of realistic models for normal and compressed a-SiO_2. This was accomplished using a Keating-type potential in the relaxation of a numerical model. The second part consists of calculations of the electronic structures of these models using the first-principles orthogonalized linear combination of atomic orbitals (LCAO) method. The last part is the calculation of the vibrational spectra of the normal and compressed a-SiO_2 models. Both the infrared and Raman spectra are calculated using the same models and the results are evaluated and discussed with respect to the CRN and paracrystalline theories. We believe this to be the first systematic calculation of both the electronic and vibrational structures of the a-SiO_2 system as a function of density. Section II outlines the methods used in the calculations and in Sec. III the results are discussed. Finally, Sec. IV summarizes the main points that are presented in this work.

II. METHODS OF CALCULATION

A. Model construction

The models for the SiO_2 glass were derived by one of us, Ching,[18] from an amorphous Si model originally constructed by Guttman.[19] All of the models discussed in this work have 162 atoms positioned in a cubic cell with periodic boundary conditions. Within the cell, the atomic configuration mimics the CRN bonding pattern as closely as possible within the limitations given. At this point, it may be advisable to defend the use of a periodic cell to model a glass system. In the silicate glass system many of the physical properties are mainly due to the local atomic environment and not the long-range periodicity. The model we used is much larger than the crystalline SiO_2 unit cell so the effect of the quasiperiodicity is negligible. Furthermore, the use of a periodic model avoids the spurious surface effects that are always present in a cluster-type calculation. In previous studies we have used similar models of silicate glasses with excellent results.[18,20–22]

The models were relaxed to a potential minimum as determined by a Keating-type potential.[22] The equations used for calculating the potentials are given in Eqs. (1)–(3):

$$V=\sum_l V_l^{\mathrm{Si}}+\sum_n V_n^{\mathrm{O}} . \tag{1}$$

Here, V_l^{Si} is the potential of the lth Si atom and V_n^{O} is the potential of the nth O atom. These potentials are defined by

$$V_l^{\mathrm{Si}}=\tfrac{3}{16}\sum_i \frac{\alpha}{d_i^2}(|\mathbf{r}_{li}|^2-d_i^2)^2 + \tfrac{3}{8}\sum_{i,i'} \frac{\beta_1}{d_i d_{i'}}(\mathbf{r}_{li}\cdot\mathbf{r}_{li'}-d_i d_{i'}\cos\phi)^2 , \tag{2}$$

$$V_n^{\mathrm{O}}=\tfrac{3}{16}\sum_i \frac{\alpha}{d_i^2}(|\mathbf{r}_{ni}|^2-d_i^2)^2 + \tfrac{3}{8}\sum_{i,i'} \frac{\beta_2}{d_i d_{i'}}(\mathbf{r}_{ni}\cdot\mathbf{r}_{ni'}-d_i d_{i'}\cos\theta)^2 . \tag{3}$$

The first term in Eqs. (2) and (3) is the bond-stretching potential summed over the nearest-neighbor (NN) atoms with which the atoms are covalently bonded. For Si the sum is over the four NN oxygen atoms. The constant, d_i, is the "ideal" Si—O bond length. To be consistent with amorphous experimental results we chose d_i to be 1.62 Å. The second term in Eq. (2) is the O—Si—O bond-bending potential. The ideal angle, ϕ, for tetrahedral bonding is 109.4°. The second term in Eq. (3) is the Si—O—Si bond-bending potential and the ideal angle is θ. In these calculations θ was chosen to be 147.0°, similar to the corresponding angle in a-SiO_2. The constants α, β_1, and β_2 determine the relative strengths of the different potential terms. The values $\alpha=1.0$, $\beta_1=0.08$, and $\beta_2=\beta_1/3$ were used in this work. These parameters are close to those used by Ching in an earlier calculation[22] of a-SiO_2 and were chosen to give optimal results for the normal density model. Generally speaking, the potential given by Eq. (1) tends to preserve the integrity of an approximate SiO_4 tetrahedral coordination by allowing a wide distribution of bridging angles θ.

The compressed a-SiO_2 models were constructed in a slightly different manner. Because the ideal Si—O bond distance in the compressed glass was not exactly known, the relaxation program allowed it to change. First the cell length parameters were reduced to achieve the desired increase in density and the model was relaxed using $d=1.62$ Å. Then the mean Si—O distance in the model was calculated and this value was used as d in a new relaxation calculation. This process was repeated until convergence was obtained. Models representing density increases of 5%, 10%, 15%, and 20% were constructed and used in the electronic and vibrational studies.

B. Electronic-structure calculations

The electronic calculations were performed using the orbital-charge self-consistent orthogonalized linear combination of atomic orbitals (OLCAO) method. This method is ideal for this work because of its accuracy and efficiency. The OLCAO method reduces the dimension of the secular equations substantially which is important for large systems.[21] This method has been well documented in the literature and we will not repeat the treatment here.[23,24] The quantities calculated include the electronic density of states (DOS), the partial density of states (PDOS), the effective valence charges (using the Mulliken method[25]), and the localization index (LI).[22] The LI is a measure of the extent to which the one-electron wave function is spread among the atoms in the model, and is a very important quantity relevant to amorphous materials. The LI $\mathcal{I}_n^{\rm loc}$ is calculated from the one-electron eigenvectors of the system according to

$$\mathcal{I}_n^{loc}=\sum_{i,\alpha}(\rho_{i\alpha}^n)^2 \ . \tag{4}$$

Here $\rho_{i\alpha}^n$ is the orbital charge i of atom α for the nth eigenvector. If the wave function is completely localized on one orbital of one atom, then $\mathcal{I}$ is equal to 1. If the wave function is completely delocalized (spread evenly over the entire model), then $\mathcal{I}$ is equal to 1 divided by the total number of orbitals in the model. For this work this means that $\frac{1}{648}<\mathcal{I}<1$. In 1958 Anderson,[26] using a simple one-band model, argued that for disordered solids of infinite extent, the states near the band edges should be highly localized while the states near the center of the band should be delocalized. Although his paper dealt with the total wave function in a fluctuating potential, the results of our finite calculations on a real system show similar patterns and can be similarly interperted.

C. Vibrational-structure calculations

The basic vibrational calculations to find the eigenvalues and normal modes of the models were accomplished using classical harmonic-oscillator techniques.

Bell *et al.*[27–31] have made a systematic effort over the years to apply the methods of vibrational analysis to the peculiarities of SiO_2. Their work proved invaluable in studying the vibrational effects in the present models. The starting point in the vibrational calculations are the Lagrange equations and the eigenvalue problem is set up as follows.

The Lagrange equation is

$$\frac{d}{dt}\frac{\partial L}{\partial \dot{q}_k}-\frac{\partial L}{\partial q_k}=0 \ , \tag{5}$$

where $L=T-V$. T is kinetic energy and V is potential energy. These are given by

$$T=\tfrac{1}{2}\sum_{k,l}M_{lk}\dot{x}_1\dot{x}_k \ , \tag{6}$$

$$V=\tfrac{1}{2}\sum_{k,l}K_{lk}x_l x_k \ . \tag{7}$$

The x_k are generalized coordinates and the M_{lk} is the mass matrix. If the x_k are orthogonal then M_{lk} is a diagonal matrix. The K_{lk} term is

$$K_{lk}=\left.\frac{\partial^2 V}{\partial x_l\,\partial x_k}\right|_{x_1=x_2=\cdots x_f=0} \ . \tag{8}$$

Note that the K_{lk} terms are evaluated at the equilibrium x_k positions. If we represent the vector x as

$$x=Ce^{-i\omega t} \tag{9}$$

then the Lagrange equations are solved by setting the following determinant to zero:

$$\det\begin{vmatrix} K_{11}-\omega^2M_{11} & \cdots & K_{1f}-\omega^2M_{1f} \\ \vdots & \ddots & \vdots \\ K_{f1}-\omega^2M_{f1} & \cdots & K_{ff}-\omega^2M_{ff}\end{vmatrix}=0 \ . \tag{10}$$

This is solved for $\omega_1,\omega_2,\cdots,\omega_f$. If the system is in equilibrium at a potential energy minimum then the ω_i values are greater than zero.

It is sometimes convenient to define a new vector, **y**:

$$y_k=M_k^{1/2}x_k \ . \tag{11}$$

Now,

$$T=\tfrac{1}{2}\sum_k \dot{y}_k^{\,2} \ , \tag{12}$$

$$V=\tfrac{1}{2}\sum_{l,k}W_{kl}y_k y_l \ , \tag{13}$$

where

$$W=\frac{K_{kl}}{M_k^{1/2}M_l^{1/2}} \ . \tag{14}$$

This makes the eigenvalue problem equivalent to solving

$$\sum_l(W_{kl}-\omega_i^2\delta_{kl})a_l^i=0, \quad k=1,2,\ldots,f \ . \tag{15}$$

This yields ω_i values which are used to get the ratios of the a_l^i. Then these must be normalized so that

$$\sum_i |a_l^i|^2=1 \ . \tag{16}$$

The simplest quantity to examine, as in the electronic calculations, is the vibrational density of states (VDOS). These curves are generated by plotting the number of vibrational states per energy unit. This can be done using only the vibrational eigenstate energies. If one wants to look at the actual movement of atoms in the solid, this requires the eigenvectors. The atomic movement in real space is given by the vectors x_k:

$$M_k^{1/2}x_k=y_k=\sum_i a_k^i e^{-i\omega_i t} \ , \tag{17}$$

$$x_k=M_k^{-1/2}\sum_i a_k^i e^{-i\omega_i t} \ . \tag{18}$$

The Keating potentials of Eqs. (1)–(3) were used in the potential energy matrix elements. It was found that the values for the weighting constants which gave the best positions for the vibrational peaks with respect to the ex-

perimental data were as follows: $\alpha=371$ N/m, $\beta_1=0.14\alpha$, and $\beta_2=0.06\alpha$. The methods for transforming the normal modes into infrared and Raman spectra were also given by Bell and Dean *et al.*[27–31]

Once the eigenvalue problem of finding the natural frequencies and the normal modes has been solved, the quantum-mechanical mechanism of electromagnetic absorption and scattering must be evaluated with regards to the vibrational motion. The derivation of this interaction can be found in the work of Bell[31] or in the reference texts which deal with vibrational spectroscopy[32–36]. For infrared light, the absorption interaction potential is u, the intrinsic dipole moment of the system. The u can be expanded to show the dependence of the atomic displacements as

$$u_\alpha = u_\alpha^0 + \sum_{j,\beta} \left. \frac{\partial u_\alpha}{\partial x_{j\beta}} \right|_{\text{at equilibrium}} x_{j\beta} + \cdots , \tag{19}$$

where u_α is the Cartesian component of u and $x_{j\beta}$ is the displacement of atom j in the β direction. Taking the linear term, the interaction matrix can be represented as

$$\langle E' | \mathbf{u} | E \rangle \propto \int \psi_{E'}^* \left[\sum_{j,\beta} \frac{\partial u_\alpha}{\partial x_{j\beta}} \right| x_{j\beta} \left] \psi_E \, d\mathbf{r} , \right. \tag{20}$$

where $\psi_{E'}$ and ψ_E are vibrational eigenstates. The dipole derivative strength of the ith eigenstate is

$$u_\alpha^i = \sum_{j,\beta} Q_j a_{j\beta}^i M_j^{-1/2} \left. \frac{\partial u_\alpha}{\partial x_{j\beta}} \right| , \tag{21}$$

where Q_j and M_j are the calculated effective charge and mass of atom j, and $a_{j\beta}^i$ is the ith normalized eigenvector in direction β of atom j. The electromagnetic energy absorbed in the solid, I, is proportional to[31]

$$I(\omega) \propto \sum_i g(\omega_i) |\mathbf{u}^i|^2 . \tag{22}$$

Here, $g(\omega_i)$ is the vibrational density of states for the system.

The calculations for the Raman spectra of the SiO_2 system are slightly more complex. Here the interaction potential is $\mathbf{p}$, the induced dipole moment of the system.[31] We have

$$p_\sigma = \sum_{\sigma'} \alpha_{\sigma\sigma'} E_{\sigma'} . \tag{23}$$

Here p_σ is the Cartesian component of the dipole moment in the σ direction, $\alpha_{\sigma\sigma'}$ is the polarizability tensor, and $E_{\sigma'}$ is the electric field. The $\alpha_{\sigma\sigma'}$ can be expanded as

$$\alpha_{\sigma\sigma'} = \alpha_{\sigma\sigma'}^0 + \sum_{j,\beta} \alpha_{\sigma\sigma'}^{j\beta} x_{j\beta} + \cdots , \tag{24}$$

so the polarizability tensor for the ith eigenstate is

$$\alpha_{\sigma\sigma'}^i = \sum_{j,\beta} a_{j\beta}^i M_j^{-1/2} \left. \frac{\partial \alpha_{\sigma\sigma'}}{\partial x_{j\beta}} \right| \tag{25}$$

which is similar to Eq. (21) for the infrared method. At this point Bell introduced the bond polarizability approximation, which relates the atomic displacements to the polarizability tensor. The atomic movements are reduced to the vector $\mathbf{R}_{kj}$ which joins atom i with all the atoms it bonds to. That is,

$$\mathbf{R}_{kj} = \mathbf{r}_{kj} + (\mathbf{x}_j - \mathbf{x}_k) , \tag{26}$$

where $\mathbf{r}_{kj}$ is the equilibrium vector from k to j and $\mathbf{x}_k$ is the movement of atom k. Now let $\hat{\mathbf{R}}_{kj}$ be the unit vector of $\mathbf{R}_{kj}$ and 1 be the unit dyadic. Then

$$\alpha_{\sigma\sigma'}(\mathbf{R}_{kj}) = [\,\overline{A}(R_{kj})\mathbf{1} + \gamma(R_{kj})(\hat{\mathbf{R}}_{kj}\hat{\mathbf{R}}_{kj} - \tfrac{1}{3}\mathbf{1})]_{\sigma\sigma'} \tag{27}$$

describes the polarizability tensor with the mean polarizability $\overline{A}(R_{kj})$ and anisotropy $\gamma(R_{kj})$. Expanding $\alpha_{\sigma\sigma'}$ in a Taylor series and keeping the linear term yields[31]

$$\begin{aligned} \sum_{j,\beta} \alpha_{\sigma\sigma'}^{j\beta} x_{j\beta} = \sum_{k,j} \{ & A'(r_{kj})[(\mathbf{x}_j - \mathbf{k}_k)\cdot\hat{\mathbf{r}}_{kj}]\mathbf{1} + \gamma'(r_{kj})[(\mathbf{x}_j - \mathbf{x}_k)\cdot\hat{\mathbf{r}}_{kj}][(\hat{\mathbf{r}}_{kj}\hat{\mathbf{r}}_{kj}) - \tfrac{1}{3}\mathbf{1}] \\ & + r_{kj}^{-1}\gamma(r_{kj})[(\mathbf{x}_j - \mathbf{x}_k)\hat{\mathbf{r}}_{kj} + \hat{\mathbf{r}}_{kj}(\mathbf{x}_j - \mathbf{x}_k) - 2(\mathbf{x}_j - \mathbf{x}_k)\cdot\hat{\mathbf{r}}_{kj}(\hat{\mathbf{r}}_{kj}\hat{\mathbf{r}}_{kj})]\}\sigma\sigma' , \end{aligned} \tag{28}$$

where $\overline{A}'$ and γ' are the derivatives of $\overline{A}$ and γ at the equilibrium positions. The parallel and perpendicular Raman scattering intensities are[31]

$$I_\parallel(\omega) \propto \sum_i g(\omega_i)(7\gamma_i^2 + 45\overline{A}_i^2)/\omega_i . \tag{29}$$

$$I_\perp(\omega) \propto \sum_i g(\omega_i)(6\gamma_i^2)/\omega_i , \tag{30}$$

in which ω_i is the eigenfrequency and the $\overline{A}$ and γ are the invariants of the polarizability tensor:

$$\overline{A}_i = \tfrac{1}{3}(\alpha_{11}^i + \alpha_{22}^i + \alpha_{33}^i) , \tag{31}$$

$$\begin{aligned} \gamma_i^2 = {} & \tfrac{1}{2}[(\alpha_{11}^i - \alpha_{22}^i)^2 + (\alpha_{22}^i - \alpha_{33}^i)^2 + (\alpha_{33}^i - \alpha_{11}^i)^2] \\ & + 3[(\alpha_{12}^i)^2 + (\alpha_{23}^i)^2 + (\alpha_{31}^i)^2] . \end{aligned} \tag{32}$$

In the present work we have used the following parameters in the Raman calculations: $\alpha'=0.9$, $\gamma=0.3$, and $\gamma'=0$. These were determined to give the best fit to the experimental data.

III. RESULTS

A. Atomic structure

The structural information on our compressed a-SiO_2 models is given in Table I. It appears that the only significant change that occurs as the models are compressed and relaxed is that the mean Si—O—Si angles get smaller. It is interesting that the mean Si—O bond does not change while the Si—O—Si angle does. This means that the compression mechanism for denser

TABLE I. Compressed SiO_2 models.

Density increase (%)	Si—O bond (Å) mean	STD	O—Si—O angle (deg) mean	STD	Si—O—Si angle (deg) mean	STD	Density (g/cm^3)
0	1.62	0.016	109.4	4.8	147.4	14.7	2.20
5	1.62	0.007	109.4	4.3	143.1	15.0	2.31
10	1.62	0.006	109.4	3.9	139.2	14.4	2.42
15	1.62	0.006	109.4	3.6	136.4	14.6	2.53
20	1.62	0.005	109.4	3.4	133.7	14.2	2.64

packing in the compressed models is a folding of the SiO_4 units about their shared corners, and not a distortion of the basic tetrahedral unit. The same type of folding mechanism has been reported for the low-temperature crystalline phase (α-quartz) of SiO_2.[37] The radial-distribution-function (RDF) curves for the five models are plotted in Fig. 1. All of the curves for $R < 3.5$ Å are very similar except that the Si—Si peak broadens and shifts from 3.14 Å in the normal density model to 3.00 Å in the model with 20% increased density. This is indicative of the decrease in the mean Si—O—Si angle with compression. For $R > 3.5$ Å, the RDF varies in a rather complicated manner, suggesting a considerable change in the intermediate range order for the compressed a-SiO_2 models. The RDF peak positions for the five models as well as relevant experimental results[16,17] are listed in Table II. The available experimental results in this range of densities are almost exactly the same as those of our models. It is obvious that the folding of the SiO_4 units seen in the models is representative of what is really happening in the a-SiO_2 system, at least up to a density increase of 16%. A point should be made at this point about the experimental results listed for the increased density SiO_2 glass. Due to experimental difficulties, all of the reported results are based on densified samples. That is, the samples were densified first and then the experimental measurements were performed at zero applied pressure. However, the glass models used in our calculations were not densified, only compressed, and the atomic positions relaxed. Despite these differences there is a strong correlation between the experimental and modeled atomic structures.

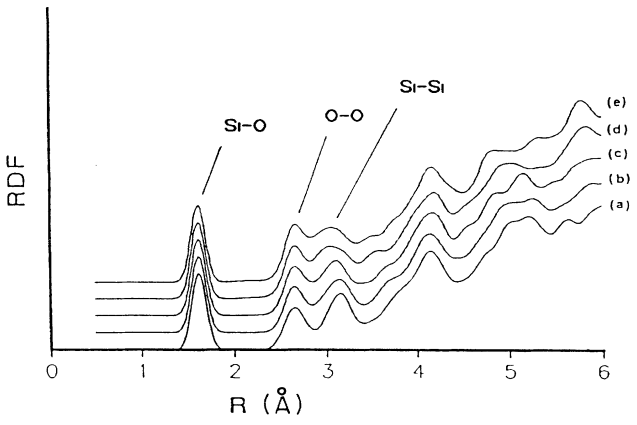

FIG. 1. Calculated RDF for compressed a-SiO_2 models. (a) normal density, (b) 5% density increase, (c) 10% density increase, (d) 15% density increase, (e) 20% density increase.

The atomic structure of this system has also been modeled using the molecular-dynamics (MD) method. Garofalini[38] has had good results in modeling silicate glass systems. However, in the modeling of a 15-kbar pressure applied to a-SiO_2, he found no change in the RDF curve and no change in Si—O—Si bond angles. An applied pressure of 15 kbar is roughly equivalent to the pressure necessary for a 5% density increase in a-SiO_2 (see Table III), and for this pressure we found that the mean Si—O—Si angle had been reduced by 4.3°. Although no experimental work on a-SiO_2 has been done at this density, the corresponding angle in α quartz decreases by 2.8° under 14.6 kbar of applied pressure.[37] Another group, Woodcock *et al.*,[39] has also attempted to model pressurized a-SiO_2. They were able to densify the a-SiO_2 model by bringing the model volume down and then back up. However, the RDF was found to be unrealistically distorted.

B. Electronic structure

The electronic structures for the five a-SiO_2 models were calculated by the first-principles OLCAO method as described earlier. The calculated band gaps for the five models are listed in Table IV. As the density increases, the band gap gets smaller, starting at 8.47 eV for the uncompressed model and dropping to 8.13 eV for the 20% increased density model. Verification of the band-gap variation as well as other results of the electronic-structure calculations for the compressed models is difficult because of the scarcity of relevant experimental work in the literature. Most of the existing experimental results concern the infrared or Raman spectra of a-SiO_2. There is one ultraviolet absorption plot in an article by Mackenzie[11] from which the band gaps can be roughly estimated. Although the exact gap is hard to determine because of the extended nature of the absorption edge, the results clearly show the gap of the densified sample to be smaller than that of the normal-density sample in agreement with our calculation.

The total electronic DOS for the normal and compressed models are presented in Fig. 2. The features of the normal-density model, Fig. 2(a), consist of three major bands. The two bands at energies less than 0 eV are the valence bands (VB). The lower VB (at -17.4 eV) is primarily due to O 2s orbitals while the upper VB (peak

TABLE II. Calculated and experimental results for compressed SiO_2 glass.

	Density change (%)	Si—O peak (Å)	O—O peak (Å)	Si—Si peak (Å)	O—Si—O angle (deg)	Si—O—Si angle (deg)
This work	0	1.62	2.65	3.14	109.4	147.4
McMillan[a]	0	1.62	2.64	3.07		142.0
This work	5	1.62	2.64	3.10	109.4	143.1
This work	10	1.62	2.64	3.07	109.4	139.2
This work	15	1.62	2.64	3.02	109.4	136.4
McMillan[a]	16	1.62	2.64	3.02		137.0
Devine[b]	16					138.0
This work	20	1.62	2.64	3.00	109.4	133.7

[a]Reference 16.
[b]Reference 17.

position -1.5 eV) is from the O $2p$ orbitals. The band with positive energy (peak at 16.1 eV) is the conduction band (CB) and is due to Si $3s$ and Si $3p$ terms. Note that the O $2p$ VB has two components. The main peak at -1.5 eV is associated with the O lone pair orbitals (nonbonding). The smaller peak at -5.0 eV is due to O—Si bonding orbitals. All of the peaks found in the uncompressed model DOS are reproduced in the curves of the compressed models. However, there are some subtle differences in the location and width of the peaks. As the compression increases, the bands get wider with a concomitant reduction in band gaps. The nonbonding orbital peaks remain constant at -1.5 eV. The CB and O $2s$ peaks move away from the top of the VB (taken to be the Fermi energy), as the density is increased. The O $2p$ VB bonding peak moves closer to the Fermi energy (and closer to the nonbonding peak) with increasing compression. Two interesting observations merit comments here. First, the three main DOS bands shown in Fig. 2 are getting wider even though the standard deviations of the bond lengths and bond angles in the model get smaller with increasing density. This means that the electronic orbital energies are being spread by the compaction process, even though the local atomic bonding configurations are not. The second point is that the compression appears to merge the bonding and nonbinding states. This may be related to the decrease in the mean Si—O—Si angles. The mean Si—O—Si angle for the normal density model is 147.4° and it reduces to 133.7° for the model with 20% increased density. This squeezing of the bonding orbitals results in increased overlap of the wave functions. This changes the charge-density distribution in this region and thus shifts the energy levels.

Also affected by the density changes in the models is the calculated effective atomic valence charges which are listed in Table IV. The Si atoms acquire more charge and the O atoms less charge as the density increases. This, too, may be caused by the redistribution of valence charges in response to the changes in the Si—O—Si mean angles.

The results of the localization index for the models are plotted in Fig. 3. If we look at Fig. 3(a) for the normal-density model, the LI behavior of the O $2s$ and the CB bands is exactly as predicted by Anderson.[26] The states at the band edges are highly localized while those in the center are relatively delocalized. However, the O $2p$ band (the middle band) does not appear to follow this rule. Actually the O $2p$ band is made up of two bands corresponding to bonding and nonbonding orbitals which slightly overlap. The peak near the center of the O $2p$ band is the consequence of the overlap of two localized band edges. When the LI of the compressed models are examined, two changes are noticed. First, the peak at the center of the O $2p$ band decreases. This supports our earlier contention that the bonding and nonbonding bands tend to merge during compression. Second, the top of the CB becomes more localized with increasing density. The CB in these models is mostly due to the Si orbitals so

TABLE III. Estimated pressures for compressed SiO_2 glass models (Ref. 13).

Density change (%)	Density (g/cm^3)	Pressure (kbar)	Pressure (GPa)
0	2.20	0	0
5	2.31	13.5	1.35
10	2.42	28.3	2.83
15	2.53	46.3	4.63
20	2.64	?	?

TABLE IV. Calculated band gaps and valence charges for compressed glass models.

Density change (%)	Band gap (eV)	Q_{Si}	Q_O
0	8.47	0.93	7.54
5	8.46	0.95	7.53
10	8.42	0.97	7.52
15	8.30	0.98	7.51
20	8.13	0.99	7.50

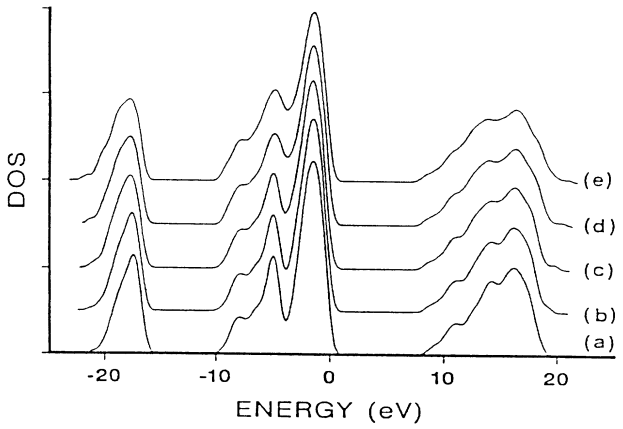

FIG. 2. Calculated DOS of compressed models. (a) normal density, (b) 5% density increase, (c) 10% density increase, (d) 15% density increase, (e) 20% density increase.

the changes in the Si—O—Si angles or the Si—Si separation distances may contribute to the LI increase.

C. Vibrational structure

The vibrational DOS (VDOS) was calculated for the five models using the Keating-type potential described earlier. The calculated VDOS of normal density SiO_2 glass is compared with the inelastic neutron-scattering results of Leadbetter and Stringfellow[40] in Fig. 4. The experimental plot shows major peaks at approximately 360 cm^{-1}, 800 cm^{-1}, and a broad peak from 950 to 1250 cm^{-1}. In comparison, the calculated VDOS shows the same three major peaks (although the position of the high-energy band is too high). In addition to the major bands, some of the smaller structures are reproduced in the calculated curve. These include the shoulder at 200 cm^{-1} and the subpeak at 565 cm^{-1}. Overall the results are in good agreement with experiment and better than Bell *et al.*[41] (who used an unrelaxed model with free or fixed surface atoms) for the low-frequency band. This may be due to the use of relaxed periodic models in the present calculations. Vibrational calculations by Guttman and Rahman[42] using a different periodic model and a modified Keating potential also produced good results for the VDOS. They obtained good position and shape for the high-energy band (including peak splitting), however, the peak position of the middle and lower bands are slightly off. The difficulty in getting all three bands in the correct positions is probably due to the failure of the Keating potential, which is short range, to completely describe the energy of this system. Long-range Columbic effects and anharmonic terms may be necessary to resolve this problem. The calculated curves and the experimental VDOS are very similar, indicating that the CRN model is adequate to describe the a-SiO_2 system.

Although other groups have modeled the normal-density SiO_2 glass with good results,[41,42] calculations on the compressed system are few. The calculated VDOS curves for the compressed models are given in Fig. 5. This figure shows that the peak at 460 cm^{-1} is stationary under pressure while the other peaks are not. The 805 cm^{-1} moves to higher wave numbers with increasing compression and the 1245-cm^{-1} peak moves to lower wave numbers. Also the subpeak at 565 cm^{-1} shows a

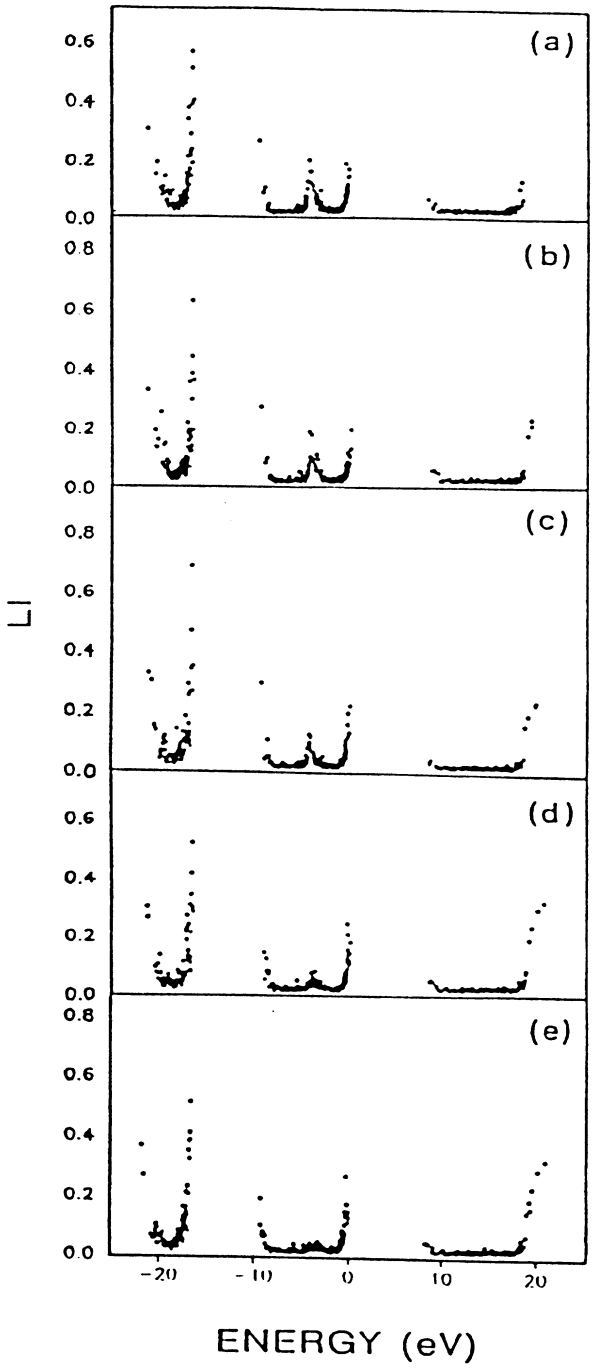

FIG. 3. Localization index for compressed SiO_2 models. Each dot represents one electronic eigenstate from the calculation. (a) normal density, (b) 5% density increase, (c) 10% density increase, (d) 15% density increase, (e) 20% density increase.

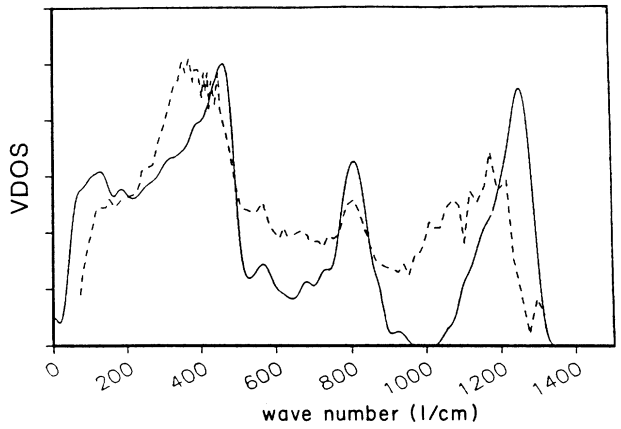

FIG. 4. Calculated and experimental VDOS for a-SiO_2. Solid line, calculated VDOS for normal density a-SiO_2; dashed line, experimental results of Leadbetter and Stringfellow (Ref. 40).

strong density dependence. At 20% increased density it moves to 625 cm^{-1}. No experimental studies of the VDOS at different densities have been published but experimental infrared results[13,43] show similar movements in the corresponding vibrational bands.

The infrared absorption was calculated using the point-dipole approximation of Bell.[31] The charges on the atoms were taken to be the effective charges obtained from the electronic calculations. The computed ir absorption is plotted with the experimental curve of Miler[44] for normal-density SiO_2 glass in Fig. 6. The shape of the two curves is very similar and there is little doubt that the three bands at 475, 825, and 1245 cm^{-1} in the computed curve are the same bands seen in the experimental plot. Also the subpeak at 565 cm^{-1} in the model curve is present in the experimental results. Here again the positions of the calculated features for wave numbers higher than approximately 900 cm^{-1} are offset from the experimental results. This is true in all of the calculated results of our models. The discrepancy may be attributed to deficiencies of the potential which were discussed earlier.

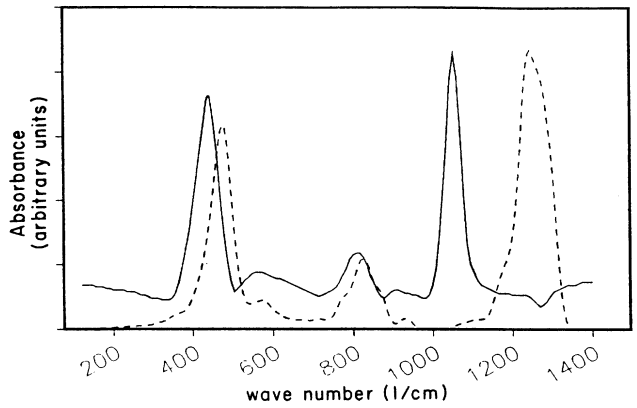

FIG. 6. Calculated and experimental infrared absorption for a-SiO_2. Solid line, experimental; dashed line, calculated.

The ir absorption for the compressed models is shown in Fig. 7. The behavior with increasing pressure is similar to that found for the VDOS. The peak at 475 cm^{-1} does not move, but the 825-cm^{-1} peak in the 0% compression model shifts to 870 cm^{-1} in the 20% compression. The peak at the 1245 cm^{-1} band shifts to lower wave numbers with increasing pressure and the peak splits. Also, the subpeak at 565 cm^{-1} moves to 625 cm^{-1} in the 20% increased-density model. The shift to higher frequencies with density for the middle band was seen experimentally by Ferraro *et al.*[43] who also saw a slight movement of the low-frequency peak. The shift to lower frequencies with increasing density of the 1245 cm^{-1} peak was reported by Cohen and Roy.[13] Both of these studies were for densified samples. Recently Velde and Count[45] have taken infrared absorption measurements of a-SiO_2 pressurized up to 29 kbar, which is below the densification threshold. They reported positive shifts

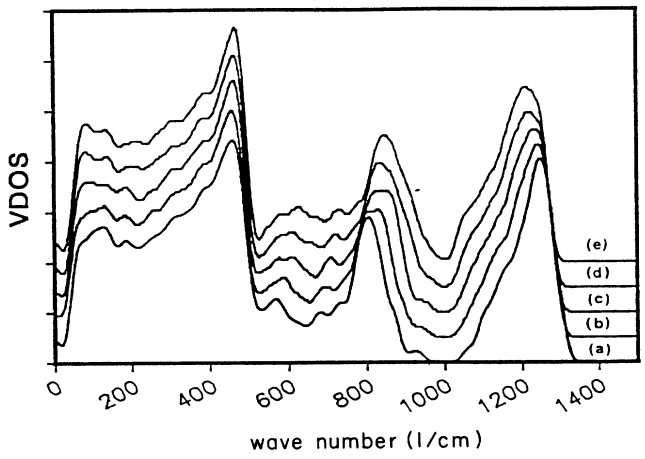

FIG. 5. VDOS of compresed a-SiO_2 models. (a) normal density, (b) 5% density increase, (c) 10% density increase, (d) 15% density increase, (e) 20% density increase.

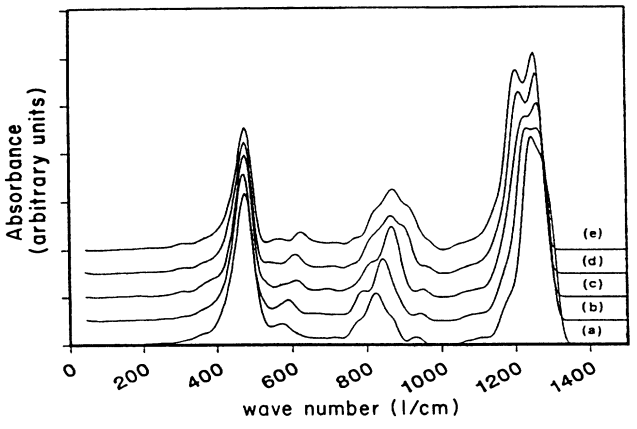

FIG. 7. Infrared absorption for compressed a-SiO_2 models. (a) normal density, (b) 5% density increase, (c) 10% density increase, (d) 15% density increase, (e) 20% density increase.

in the position of the 500-, 800-, and 1000-cm^{-1} bands with increasing pressure. From this, it would appear that the movement of the 1000-cm^{-1} band depends on whether the sample is irreversibly changed (densified) or simply compressed. However, the results of Hemley *et al.*[46] on the Raman spectra of compressed samples seem to contradict this conclusion, at least for this pressure range. This will be discussed in more detail later. It is clear that although the absolute peak positions of our calculations are not in perfect agreement with experiment, they are quite close and the trend of the movement of the peak positions with density changes is in good agreement with experimental measurement.

The Raman spectra are a sensitive tool for studying the atomic structure of a-SiO_2. However, the Raman spectra alone cannot be used to determine the atomic bonding patterns for this system. Recently, it has been used as the main evidence in the controversy over the long-range structure of a-SiO_2. Phillips[8] has asserted that certain peaks in the Raman spectra at 495 and 606 cm^{-1} are evidence that the continuous-random-network (CRN) theory of silicate glass is incorrect. He formulated a paracrystalline theory which states that the a-SiO_2 structure is actually large (>30 Å diameter) clusters of crystalline β-cristoballite[8] separated by unspecified material with higher defect concentrations than the clusters. Within this structure there exist two types of NBO sites. The first type, called D_1, gives rise to the structure at 495 cm^{-1} and occurs at the cluster surface. The second type, D_2, is a point defect and is responsible for the structure at 606 cm^{-1}. The presence of the D_1 and D_2 peaks in the parallel Raman spectra of a-SiO_2 is taken by Phillips as strong evidence in support of the paracrystal model. On the other hand, Galeener[9,10] supports the CRN model and contends that the D_1 and D_2 Raman peaks can be explained by the vibration associated with four-fold and three-fold ring structures that may exist in the glass network. These are atoms connected in rings by covalent bonding containing four or three Si atoms, respectively. The Raman spectra of normal and densified a-SiO_2 have been interpreted in support of both theories in the past several years[12,16,46] and it was hoped that our calculations on the normal and compressed models would help to resolve this controversy.

The Raman spectra were calculated using the bond polarizability approximation discussed by Bell.[31] The calculated Raman spectra for the normal-density a-SiO_2 model are plotted together with the experimental work of McMillan *et al.*[16] in Figs. 8 and 9. Figure 8 is for the perpendicular Raman spectra and, like the VDOS and infrared absorption, it consists of three major bands. In the calculated spectra they occur at 453, 800, and 1232 cm^{-1}. For the two lower-energy bands, the calculated curve is very close in peak position and peak shape to the experimental curve. Even the shoulder at 110 cm^{-1} is present and well placed. However, the calculated band at 1232 cm^{-1} is not positioned correctly with respect to the experimental curve and it fails to yield the double peaks seen by McMillan.[16] In their calculations on a smaller (12 SiO_4 units) normal-density model,[30] Bell *et al.* were able to produce the twin peaks found in the experimental

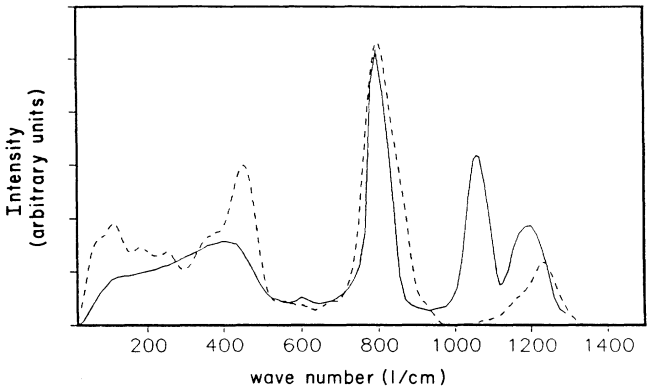

FIG. 8. Calculated and experimental perpendicular Raman spectra for a-SiO_2. Solid line, experimental results of McMillan *et al.* (Ref. 16); dashed line, calculated results.

results at 1100–1200 cm^{-1}. But, the peak position of the middle (800 cm^{-1}) band in their results is misplaced with respect to the experimental work. Again, this probably reflects some imperfections in the short-ranged Keating-type potential used. Figure 9 shows the calculated parallel Raman spectra for our normal-density model and the experimental results of McMillan.[16] The peaks marked D_1 and D_2 on the experimental curve are the "defect peaks" discussed by Phillips.[8] The spectra calculated for the normal-density a-SiO_2 model fits the low and middle bands rather well. As before, the top band is not accurately reproduced by the model. The lower-energy calculated band has some extraneous features at 182 and 291 cm^{-1} but overall it reproduces the shape and position of the experimental results. The most interesting point about the lower band is that is reproduces the D_1 and D_2 peaks found in the experimental results without NBO sites in the model. This would seem to nullify much of the evidence for the paracrystalline theory. Phillips[8] has discounted similar Raman calculations by Bell and Hibbins-Butler[29] due to the extra features in the low-energy band (peaks at 100 and 310 cm^{-1}), and also because the best agreement in their calculations came from

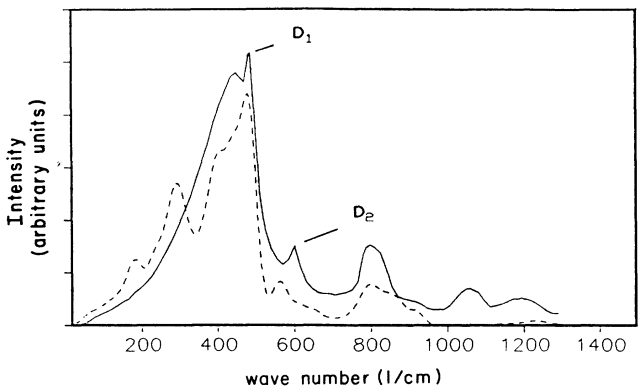

FIG. 9. Calculated and experimental parallel Raman spectra for a-SiO_2. Solid line, experimental results of McMillan *et al.* (Ref. 16); dashed line, calculated results.

TABLE V. Model ring statistics. The numbers in parentheses indicate the percentage difference the values in the D_1 and D_2 columns are from the mean numbers of ring types bonded to the Si or O atoms found in the total model.

		Model	D_1	D_2
Threefold	Si mean	0	0	0
	O mean	0	0	0
Fourfold	Si mean	0	0	0
	O mean	0	0	0
Fivefold	Si mean	2.87	4.00[a](39%)	3.10(8%)
	O mean	1.44	1.62(12%)	1.63(13%)
Sixfold	Si mean	5.22	6.00[a](15%)	4.95(−5%)
	O mean	2.61	2.46(−6%)	2.79(7%)
Sevenfold	Si mean	5.96	6.00[a](1%)	6.15(3%)
	O mean	2.98	2.92(−2%)	2.79(−6%)

[a]Contains only one Si atom.

including the surface atoms in their model as free. These free-surface atoms are effectively NBO sites. In our calculations, where none of the a-SiO_2 models have NBO atoms and the free surface has been circumvented by the periodic boundaries, the D_1 and D_2 features still appear. In the normal-density a-SiO_2 calculations, the D_1 and D_2 peaks occur at 477 and 561 cm^{-1}, respectively.

Demonstrating that the defect peaks can be reproduced without the presence of NBO sites may weaken the paracrystalline theory, but it does not, in itself, support the ring theory. According to Galeener,[9,10] the D_1 peak is due to planar fourfold rings and the D_2 peak is from threefold rings. Our model does not contain any threefold or fourfold rings since such structures generally result in large bond-length and bond-angle distortions. The ring statistics for the a-SiO_2 model used in the present calculations are given in Table V. This table lists the mean number of five-, six-, and sevenfold rings that are attached to the Si and O atoms in the model. Also listed are the ring statistics of the atoms participating in the D_1 and D_2 peaks as analyzed by inspection of the eigenvector components of these modes. It should be noted that the normal and compressed models have the same ring statistics because, in our study, the compression process does not change the topology of the model, only the bond lengths and angles. The most obvious point in Table V is that there are no three- or fourfold rings in the models. This means that the D_1 and D_2 peaks in the calculated Raman spectrum are not strictly due to the ring configurations as suggested by Galeener. The numbers in the second and third columns in Table V list the mean number of rings (as well as the percent difference from the entire model average) attached to Si and O atoms participating in the three eigenstates closest to the D_1 and D_2 peaks. Note that the atoms participating in the D_1 peak had only one Si atom while the atoms for D_2 were mixed. This means that the Si ring statistics for the D_1 peak should not be taken too seriously. However, by inspection of the O statistics for both peaks one concludes that the D_1 peak in the models is due to fivefold rings and the D_2 is from five- and sixfold rings. This does not mean that Galeener's approach is without support. Table VI shows the ring structures associated with the D_1 and D_2 peaks in the Galeener theory and the expected mean Si—O—Si angles. Also listed in this table are the mean Si—O—Si angles of the O atoms participating in the D_1 and D_2 peaks in our a-SiO_2 model. The mean angle for D_1 is 160.5° for the fourfold rings in Galeener's theory and 148.8° for the atoms (mostly fivefold) in our uncompressed glass model. Similarly, the mean angle associated with D_2 is 130.5° for Galeener's threefold rings and 137.8° in our uncompressed model. So, even though our uncompressed model had no three- or fourfold rings, the Si—O—Si angles are close to those predicted by Galeener. It would appear then that Galeener's theory should be generalized to account for the Si—O—Si angles instead of ring size. Larger ring sizes, that is, rings with more members, can approach the bridging angles found in Galeener's three- and fourfold rings by bending out of plane. Of course, in a real a-SiO_2 system, the presence of isolated threefold or fourfold rings cannot be ruled out.

The behavior of the total Raman spectra with increasing density is shown in Fig. 10. The low- and middle-energy bands shift to higher wave numbers and the high-energy band shifts to lower wave numbers. The lower band also becomes much sharper with increasing density. These band shifts have been reported for densified samples by McMillan *et al.*[16] Until recently all experimental Raman spectra on compressed a-SiO_2 were performed on densified samples, that is, with no applied pressure at the time of measurement. Hemley *et al.*[46] have obtained Raman results for a-SiO_2 under pressure by the diamond-

TABLE VI. Raman peaks.

	D_1 (495 cm^{-1})	D_2 (606 cm^{-1})
Phillips	NBO	NBO
Galeener	fourfold rings (160.5°)	threefold rings (130.5°)
Uncompressed model (this work)	fivefold rings (148.8°)	five- and sixfold rings (137.8°)

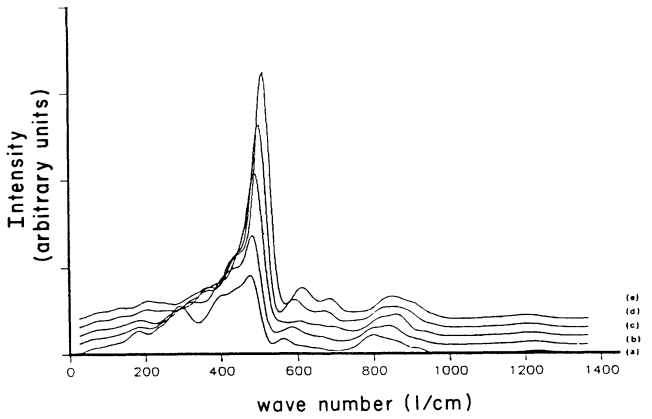

FIG. 10. Calculated total Raman spectra for compressed a-SiO_2 models. (a) normal density, (b) 5% density increase, (c) 10% density increase, (d) 15% density increase, (e) 20% density increase.

anvil technique. In going from 0.1 MPa to 8 GPa, the low-energy band went from a broad maximum at 440 cm^{-1} and the D_1 peak at 492 cm^{-1} to a very sharp, narrow peak at 530 cm^{-1}, the 800-cm^{-1} band shifted to 850 cm^{-1}, and the small peak at 1060 cm^{-1} shifted to 1052 cm^{-1}. Here the movement of the high-energy band is in the opposite direction to that found by Velde and Couty[45] for pressurized ir absorption. The Hemley group states that the changes in their sample were reversible up to approximately 9 GPa. These conflicting results introduce some uncertainty into the behavior of the high-energy band under pressure. The changes in the Raman spectra in going from our uncompressed model to the 20% increased-density model are very similar in magnitude and direction to those found by Hemley. It is not possible to estimate the effective pressure on our 20% model very closely from Table III, but it is safe to say that it is over 6 GPa. The lower band has a large feature near 440 cm^{-1} and the D_1 peak at 477 cm^{-1}. These merge into a single sharp peak at 512 cm^{-1} as the density is increased by 20% as seen in Fig. 10. At the same time the 800 cm^{-1} band shifts to 851 cm^{-1} and the peak at 1232 cm^{-1} moves to 1200 cm^{-1}. Galeener[47] and Sen and Thorpe[48] have published calculations which show that these band shifts can be correlated to decreases in the mean Si—O—Si angles with increased density. In our models the mean angles are 147.4° for normal density and 133.7° for a 20% density increase. Hemley[46] attributes the increasing sharpness of the 440-cm^{-1} band with increasing pressure to a decrease in the Si—O—Si angle distribution. However, as can be seen in Table I, the standard deviation of the Si—O—Si angles remains fairly constant at approximately 15°. The behavior of the D_1 and D_2 peaks in Fig. 10 is interesting. Both features move to positions of higher wave numbers as the density increases. This can be explained by the same mechanism that shifts the other bands, the decrease in mean Si—O—Si angle with increasing density. It appears that similar movement occurs for the D_1 peak of Hemley's pressurized a-SiO_2 results but the D_2 peak does not show a corresponding shift.

IV. CONCLUSIONS

From the results presented in the previous sections, it appears that the compressed models obtained from our calculations simulate the densified glass reasonably well. The primary change in the a-SiO_2 system with increasing density is that the mean Si—Si distance gets smaller. This was seen as a reduction in the mean Si—O—Si angles for the compressed models. Given that the Si—O bond lengths stayed essentially constant, the compaction mechanism must be a folding of the undistorted SiO_4 tetrahedra similar to that reported for α-quartz.[37] The success of the compressed models in reproducing most of the experimental results indicates that Keating-type potentials can be used to simulate covalent networks under pressure.

The calculations on the electronic structures of the compressed a-SiO_2 have shown that increasing the density of the material changes the band gaps and effective valence charges only slightly. However, the shape of the O $2p$ VB band is effected by the compression in a way that causes the bonding and nonbonding bands to overlap. This point is vividly demonstrated by the LI plots.

The vibrational-structure calculations presented the most stringent test for the compressed model structures. However, it provided an opportunity to repeat the Bell and Dean calculations with models having periodic boundaries and variable density. In general, the results were as good or better than the previous work. In particular, the calculated results for the VDOS and infrared absorption were quite good with respect to the densified samples. However, the movement of the high-energy peak in the ir with increasing density was opposite that obtained by Velde and Couty.[45]

The results for the Raman spectra are mixed. The agreement with experiment is good for the low- and middle-energy bands but the top band does not reproduce the published data well. However, contained in the low- and middle-energy curves are some important results. The D_1 and D_2 peaks in the Raman spectra were reproduced without NBO atoms in a CRN model. This is in contradiction to the paracrystalline theory of Phillips. The peaks were also formed without the three- and four-fold rings postulated by the Galeener. Inspection of the eigenvectors of the modes responsible for the D_1 and D_2 peaks and the correlation to the topological characteristics of the a-SiO_2 model indicate that the distribution of the Si—O—Si bridging angles, rather than the ring statistics, may be the relevant factor.

Overall, the calculated properties of the compressed a-SiO_2 models were very close to the experimental results. The places where the models failed, such as the high-energy vibrational bands, can be used to improve the vibrational potentials and to construct more realistic models in the future. It is anticipated that, using the approach outlined in this paper, other important and interesting work such as the study of defects and impurities in glasses may be undertaken in the near future.

ACKNOWLEDGMENT

This work was supported by U.S. Department of Energy, Grant No DE-FG02-84ER45170.

*Present address: U. S. Army Laboratory Command (SLCET-EQ), Fort Monmouth, NJ 07703-5302.

[1]B. E. Warren, H. Krutter, and O. Morningstar, J. Am. Ceram. Soc. **19**, 202 (1936).
[2]W. H. Zachariasen, J. Am. Chem. Soc. **54**, 3841 (1932).
[3]G. Hägg, J. Chem. Phys. **3**, 42 (1935).
[4]B. E. Warren and J. Biscoe, J. Am. Ceram. Soc. **21**, 259 (1938).
[5]E. A. Porai-Koshits, *The Structure of Glass* (Consultants Bureau, New York, 1950), p. 25.
[6]Y. Waseda and H. Suito, Iron Steel Inst. Jpn. **17**, 82 (1977).
[7]M. Misawa, D. L. Price, and K. Suzuki, J. Non-Cryst. Solids **37**, 85 (1980).
[8]J. C. Phillips, in *Solid State Physics,* edited by H. Ehrenreich, F. Seitz, and D. Turnbull (Academic, New York, 1982), Vol. 37, p. 93.
[9]F. L. Galeener, Solid State Commun. **44**, 1037 (1982).
[10]F. L. Galeener and A. C. Wright, Solid State Commun. **57**, 677 (1987).
[11]J. D. Mackenzie, J. Am. Ceram. Soc. **46**, 461 (1963).
[12]M. Grimsditch, Phys. Rev. Lett. **52**, 2379 (1984).
[13]H. M. Cohen and R. Roy, Phys. Chem. Glasses **6**, 149 (1965).
[14]M. Grimsditch, Phys. Rev. B **34**, 4372 (1986).
[15]S. Sakka and J. D. Mackenzie, J. Non-Cryst. Solids. **1**, 107, (1969).
[16]P. McMillan, B. Piriou, and R. Couty, J. Chem. Phys. **81**, 4234 (1984).
[17]R. A. B. Devine and J. Arndt, Phys. Rev. B **35**, 9376 (1987).
[18]W. Y. Ching, in *Proceedings of the International Topical Conference on the Physics of MOS Insulators, Raleigh, 1980,* edited by G. Lucovsky, S. T. Pantelides, and F. L. Galeener (Pergamon, New York, 1980).
[19]L. Guttman, Bull. Am. Phys. Soc. **22**, 64 (1977).
[20]R. A. Murray, L. W. Song, and W. Y. Ching, J. Non-Cryst. Solids **94**, 133 (1987).
[21]R. A. Murray and W. Y. Ching, J. Non-Cryst. Solids **94**, 144 (1987).
[22]W. Y. Ching, Phys. Rev. B **26**, 6610 (1982); Phys. Rev. Lett. **46**, 607 (1981).
[23]W. Y. Ching and C. C. Lin, Phys. Rev. B **12**, 5536 (1975).
[24]W. Y. Ching and C. C. Lin, Phys. Rev. B **16**, 2989 (1977).
[25]R. S. Mulliken, J. Chem. Phys. **23**, 1833 (1955).
[26]P. W. Anderson, Phys. Rev. **109**, 1492 (1958).
[27]R. J. Bell and P. Dean, Nature (London) **212**, 1354 (1966).
[28]R. J. Bell and P. Dean, Discuss. Faraday Soc. **50**, 55 (1970).
[29]R. J. Bell and D. C. Hibbing-Butler, J. Phys. C **9**, 1171 (1976).
[30]R. J. Bell, A. Carnevale, C. R. Kurkjian, and G. E. Peterson, J. Non-Cryst. Solids **35-36**, 1185 (1980).
[31]R. J. Bell, *Methods in Computational Physics* (Academic, New York, 1976), Vol. 15, p. 215.
[32]D. Steele, *Theory of Vibrational Spectroscopy* (Saunders, Philadelphia, 1971), p. 114.
[33]E. B. Wilson, Jr., J. C. Decius, and P. C. Cross, *Molecular Vibrations* (McGraw-Hill, New York, 1955), p. 289.
[34]S. Califano, *Vibrational States* (Wiley, New York, 1976), p. 1.
[35]L. A. Woodward, in *Raman Spectroscopy,* edited by H. A. Szymanski (Plenum, New York, 1967), p. 1.
[36]G. Zerbi, in *Vibrational Intensities in Infrared and Raman Spectroscopy,* edited by W. B. Person and G. Zerbi (Elsevier, New York, 1982), p. 51.
[37]J. D. Jorgensen, J. Appl. Phys. **49**, 5473 (1978).
[38]S. Garofalini, J. Chem. Phys. **76**, 3189 (1982).
[39]L. V. Woodcock, C. A. Angell, and P. Cheesman, J. Chem. Phys. **65**, 1565 (1976).
[40]A. J. Leadbetter and M. W. Stringfellow, in *Neutron Elastic Scattering, Proceedings of the International Atomic Energy Agency, Grenoble* (IAEA, Vienna, 1972), p. 501.
[41]R. J. Bell, N. F. Bird, and P. Dean, J. Phys. C **1**, 299 (1968).
[42]L. Guttman and S. Rahman, J. Non-Cryst. Solids **75**, 419 (1985).
[43]J. R. Ferraro, M. H. Manghnani, and A. Quattrochi, Phys. Chem. Glasses **13**, 116 (1972).
[44]M. Miler, Czech. J. Phys. B **18**, 354 (1968).
[45]B. Velde and R. Couty, J. Non-Cryst. Solids. **94**, 238 (1987).
[46]R. J. Hemley, H. K. Moa, P. M. Bell, and B. O. Mysen, Phys. Rev. Lett. **57**, 747 (1986).
[47]F. L. Galeener, Phys. Rev. B **19**, 4292 (1979).
[48]P. N. Sen and M. F. Thorpe, Phys. Rev. B **15**, 4030 (1977).